

Tracing the boron diffusion into a textured silicon solar cell by combining boron diffusion simulation with experimental and simulated scanning transmission electron beam induced current

Tobias Meyer,¹ David A. Ehrlich,¹ Peter Pichler,^{2,3} Valeriya Titova,^{4,5}
Christoph Flathmann,¹ Jan Schmidt,^{4,5} and Michael Seibt^{1,*}

¹*4th Institute of Physics – Solids and Nanostructures,*

University of Goettingen, Friedrich-Hund-Platz 1, 37077 Göttingen, Germany

²*Fraunhofer Institute for Integrated Systems and Device Technology IISB, Schottkystrasse 10, 91058 Erlangen, Germany*

³*Universität Erlangen-Nürnberg, Lehrstuhl für Elektronische Bauelemente Cauerstrasse 6, 91058 Erlangen, Germany*

⁴*Institute for Solar Energy Research Hamelin (ISFH), Am Ohrberg 1, 31860 Emmerthal, Germany*

⁵*Institute of Solid-State Physics, Leibniz Universität Hannover, Appelstrasse 2, 30167 Hannover, Germany*

The light absorption of [001] grown single-crystalline silicon wafers can be enhanced by chemical etching with potassium hydroxide resulting in a pyramid-like surface texture. Alongside this advantageous property in the context of solar energy conversion, the surface roughness leads to drawbacks as well, e.g. difficulties in measuring diffusion behaviour of dopants in the heterogeneous structure. In this paper, we employ experimental and simulated scanning transmission electron beam induced current in combination with the simulation of boron diffusion to map a sub 0.1 ppm iso-concentration line underneath the textured surface on the nanoscale. In order to account for surface recombination, an effective two-dimensional model projecting the system along the electron beam propagation direction is used in the finite elements EBIC simulation. We find a good agreement to the experimental data and discuss future strategies to eliminate remaining deviations inside the space charge region.

I. INTRODUCTION

The theoretical limit for the efficiency of single junction crystalline silicon solar cells, also known as the Shockley-Queisser limit, amounts to approximately 30 percent [1]. Accounting only for transmission of sub-bandgap photons and thermalisation of hot carriers, this value is still significantly higher than practically achieved performances being deteriorated by e.g. enhanced excess charge carrier recombination at the contacts or reflection of the incident light [2, 3]. Thus, electrically and chemically passivated as well as textured, strongly absorbing surfaces are highly desirable. A low-cost processing step to achieve a pyramid-like surface texture and consequently high absorption of [001] silicon wafers is chemical etching [3]. Nevertheless, the surface texture can interfere with subsequent preparation steps such as the diffusion of dopants to form the solar cell's emitter layer. Unfortunately, classical methods to determine doping profiles like electrochemical capacitance voltage (ECV) measurements resp. secondary ion mass spectrometry (SIMS) become difficult in the presence of textured surfaces due to limited lateral resolution [4] resp. a decreasing elemental sensitivity for decreasing sputtering volumes [5], i.e. increasing spatial resolution. In addition, SIMS yields the elemental concentrations independent of their electrical activity being of major interest in the context of device fabrication. Alternatively, the diffusion of dopants [6], in particular boron [7, 8], in

silicon was studied extensively on planar samples to determine corresponding diffusion parameters which can be used subsequently as input parameters for the simulation of heterogeneous structures. In fact, an enhanced boron mobility in the case of an oxidizing ambience was found in [7]. The entire path of extracting diffusion parameters in a 1D model from planar samples and applying them numerically to 2D pyramid-like textured surfaces is presented in [9]. Additionally, electron beam induced current (EBIC) measurements are presented to verify the qualitative shape of the simulated isoconcentration lines.

In this work, we demonstrate how scanning transmission EBIC in combination with boron diffusion simulation can be employed to quantitatively map a sub 0.1 ppm iso-concentration line underneath a textured single-crystalline silicon solar cell on the nanoscale. As reported in [10–14], the spatial resolution of EBIC in transmission mode is superior to its conventional counterpart since the electron beam does not get spread significantly due to scattering in the sample. Clearly, surface effects become more dominant in a thin, electron transparent lamella, which is addressed by comparing the experimental data to finite element simulations (FEM) in an effective two-dimensional model. We find a good agreement between experimental and simulated maps and remaining deviations in the space charge region (SCR) are thoroughly discussed.

II. SAMPLE PREPARATION AND INSTRUMENTATION

A detailed description of the preparation process of the silicon solar cell can be found in [15]. Nevertheless,

*Electronic address: mseibt@gwdg.de

a brief summary of the main steps related to the boron diffusion process conducted in a Tempress Systems TS-81004 furnace shall be given:

1. Heat-up: The furnace temperature is increased from 700 °C to 941 °C using a ramping speed of 10 °C/min in an inert ambience.
2. Deposition: Keeping the temperature in the furnace stabilized, N₂ is lead through a liquid BBr₃ bubbler held at 20 °C leading to a B₂O₃ flow which is subsequently mixed with N₂ and O₂.
3. Drive-in: The flow through the bubbler is switched off while all other parameters remain unchanged for further 20 min.
4. Post-oxidation: The N₂ and O₂ gas flows are reduced and the temperature is held constant for further 60 min.
5. Cool-down: In an inert ambience, the temperature is decreased by -10 °C/min and the sample carrier ultimately retracted at 805 °C.

In addition to the potassium hydroxide treated textured wafer, a planar reference sample was processed simultaneously and investigated by four point probe (4PP) measurements subsequently to determine the sheet resistance of the resulting boron doped layer in the homogeneous case.

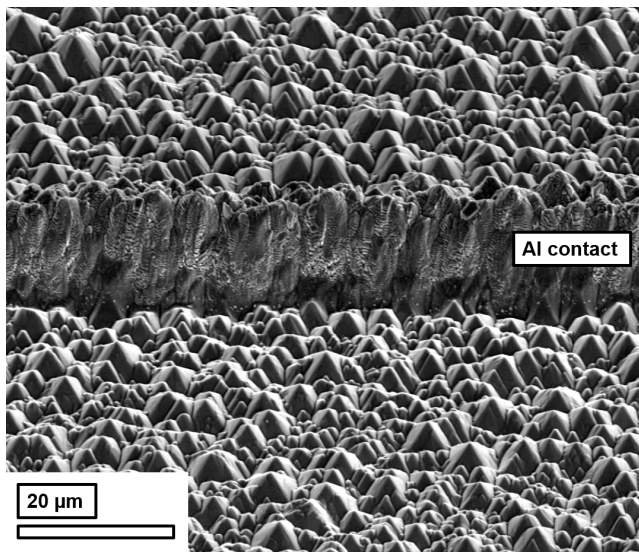


FIG. 1: SEM overview of the pyramid texture of the solar cell including an aluminium front contact. The surface is inclined by 45 degrees.

An SEM overview of the the textured surface including an aluminium front contact is shown in Fig. 1. An electron transparent lamella was extracted from the aluminium covered area using a FEI Nova NanoLab Dual Beam focused ion beam. The acceleration voltage for

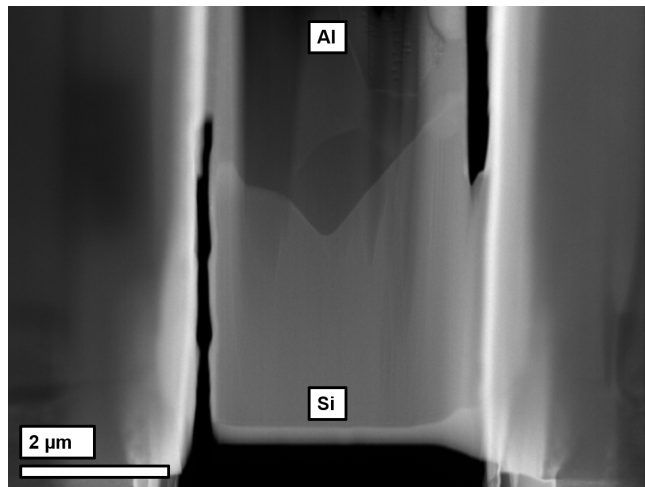


FIG. 2: ADF STEM overview of the [110] oriented lamella including a trench between two pyramids in the central region. Vertical cuts have been performed to prevent short circuits across the investigated area.

the final thinning step was decreased from 30 kV to 5 kV in order to minimize beam damage. An annular dark-field (ADF) STEM overview of the resulting lamella is shown in Fig. 2. The vertical cuts have been performed during FIB preparation to prevent short circuits across the electrical junction due to redeposited material. To allow for electrical contacting inside the scanning transmission electron microscope (STEM), a DENSSolutions Lightning D7+ holder was used. All STEM experiments were performed inside an FEI Titan80-300 operated at 300 kV. The beam current was set to 42 pA and an acceptance semi-angle of 39 mrad was used for electron energy loss spectroscopy (EELS) employing a Gatan Quantum 965 ER. The short circuit current was converted to an output voltage with a Stanford Research Systems SR570 and subsequently fed to the AD converter of the Gatan DigiScan II scan unit controlling the electron beam during the acquisitions.

III. EXPERIMENTAL RESULTS

The central part of the lamella shown in Fig. 2 including a trench between two pyramids was investigated simultaneously by ADF STEM resp. EBIC yielding the results presented in Fig. 3(a) resp. (b). Clearly, the domain of finite EBIC signals lies well below the textured surface and the shape is comparably smooth. In order to illustrate the shape of the EBIC signal across the junction, a normalized profile averaged over the four left-most columns in Fig. 3(b) is shown in Fig. 7. Including only points below 0.25 to exclude effects of the space charge region, the decaying tails of the profile on each respective side were fitted to an exponential function yielding a decay length of the EBIC signal of 83 nm resp. 136 nm on the p- resp. n-side. Correcting for the approx-

imately 40° inclination of the surface, this translates to effective diffusion lengths of 63 nm resp. 103 nm. Obviously, these values are well below those expected in bulk material indicating the strong influence of surface recombination which will be discussed later in detail. However, due to the homogeneous thickness in the EBIC domain of 1.76(4) mean inelastic free paths (determined by EELS following Malis' method [16]) which translates to approximately 342(7) nm [17], relative thickness effects on the excess charge carrier recombination can be neglected.

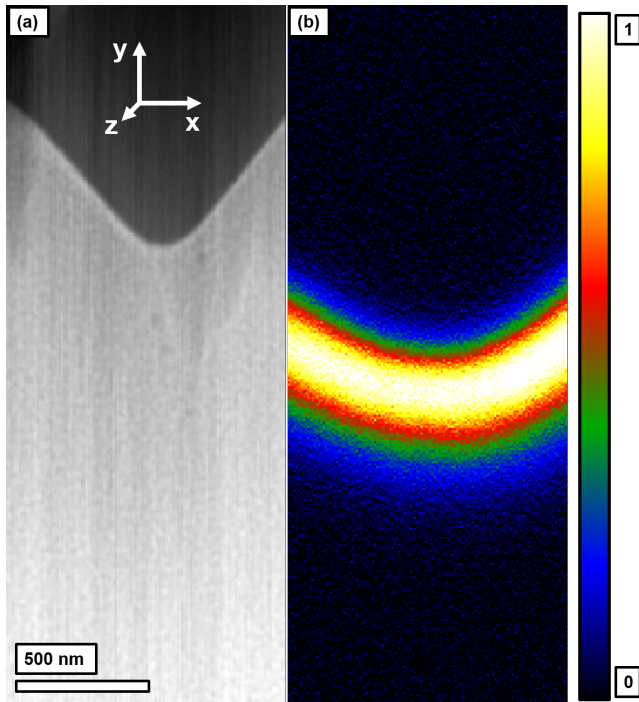


FIG. 3: (a) ADF STEM image of the central region of the lamella and (b) the corresponding EBIC map normalized to its maximum. The spatial directions used throughout the paper are indicated in (a) and the origin is set to the upper left corner in all following figures.

IV. BORON DIFFUSION SIMULATION

While sufficiently accurate models exist for the diffusion of boron in silicon, this is neither the case for the growth of boron glasses nor for the diffusion of boron in the glass or for its segregation into silicon. In lack of more detailed knowledge, the main process steps are modeled as follows: Following [18], the partial pressures of O_2 and B_2O_3 under the given conditions in the furnace are calculated yielding the growth of a thin partially liquid boron glass. The doping of the growing glass with boron is simulated using a Dirichlet boundary condition at the interface between the ambience and the glass. After the boron source is switched off, a negligible evaporation of boron into the furnace is assumed during the process steps drive-in, post-oxidation and cool-down. It has to

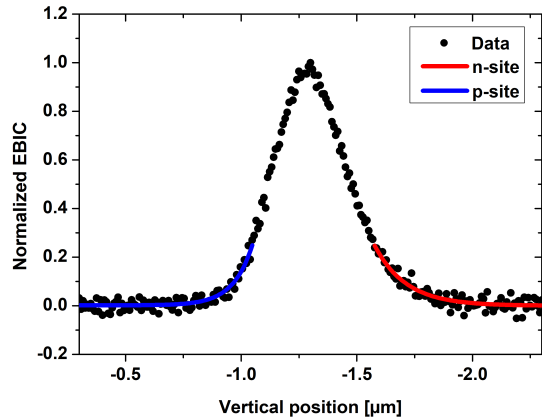


FIG. 4: Vertical EBIC profile averaged over the four left-most columns in Fig. 3(b) as well as exponential fits of the profile's tails on the n- and p-side, respectively. Only values below 0.25 have been considered during fitting.

be noted, though, that simulations with diffusion-limited evaporation and an adapted boron concentration at the interface to the ambience during the deposition step lead to very similar boron profiles. Particularly during the post-oxidation step, the boron diffuses deeply into the silicon but segregates also into the growing oxide glass. This results in a retrograde boron profile in the silicon with a maximum concentration approximately $0.12 \mu\text{m}$ below the surface.

For the numerical implementation, Sentaurus Process of Synopsys, Version Q-2019.12, was used with AdvancedCalibration and the two-phase segregation model for boron at the silicon-silicon dioxide interface. Within the simple modeling approach taken, the boron concentration at the oxide surface during the deposition step has a main influence on the final sheet concentration of boron in the silicon and thus on its sheet resistance. A second uncertainty results from the enhancement of the boron diffusion during all process steps in oxidizing atmosphere. Established models exist for the dry oxidation of silicon with low dopant concentrations in the oxide. However, the oxide glass growing here is highly doped and partially liquid which should result in considerably less strain in the glass. Following the arguments of [19], the different stress state should result also in a different injection of self-interstitials and thus oxidation enhancement.

In order to fix the boron concentration at the oxide surface during deposition as well as the degree of oxidation enhancement, two experimental observations are used: Firstly, the sheet resistance of $102 \Omega/\text{sq}$ obtained by the 4PP measurements on the planar reference sample. Secondly, the position of the chemical junction, assuming that a boron concentration of $3.5 \times 10^{15} \text{ cm}^{-3}$ coincides with the column-wise EBIC maximum underneath the tip of the trench in Fig. 3(a). Both experimen-

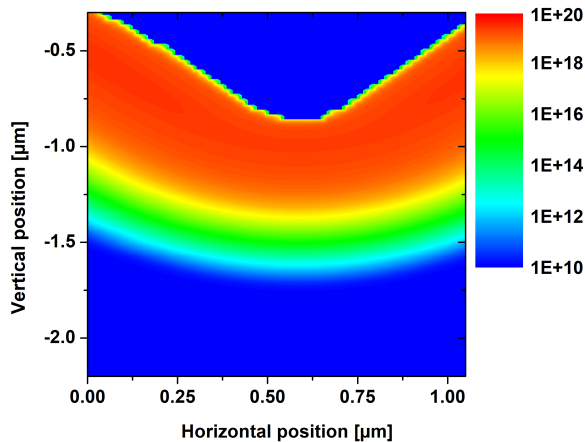


FIG. 5: Simulated two-dimensional boron concentration underneath the surface texture shown in Fig. 3(a). The numbers in the colour-code are given in cm^{-3} .

tal findings are met using an oxide surface concentration of $N_{\text{B,surface}} = 1.55 \times 10^{22} \text{ cm}^{-3}$ during the deposition and an OED scaling factor of about 0.34 leading to the two-dimensional boron distribution underneath the textured surface shown in Fig. 5. For this figure, to avoid boundary effects, the surface topography was linearly extrapolated on the left and right side by each 500 nm during the simulation and Neumann boundary conditions were assumed for the diffusion equations.

V. NUMERICAL EBIC MODEL

To simulate the drift diffusion behaviour of excess charge carriers, a 2D model (omitting the electron propagation direction, i.e. z) with three variables is used: The electrostatic potential ϕ as well as the electron and hole concentrations n and p . In addition, following parameters are needed: The ionized acceptor and donor concentrations N_{a}^- and N_{d}^+ , the relative permittivity ϵ_{r} , the electron and hole mobilities μ_{e} and μ_{h} , the intrinsic charge carrier concentration n_{i} as well as the excess charge carrier generation and recombination rates g and r . The set of partial differential equations that have to be solved is given by Poisson's equation (1) and the stationary continuity equations including sinks and sources for electrons (2) and holes (3):

$$-\vec{\nabla} \cdot (\epsilon_0 \epsilon_{\text{r}} \vec{\nabla} \phi) = e (N_{\text{d}}^+ - N_{\text{a}}^- + p - n), \quad (1)$$

$$0 = \frac{dn}{dt} = -\vec{\nabla} \cdot \left(\mu_{\text{e}} n \vec{\nabla} \phi - \frac{k_{\text{B}} T}{e} \mu_{\text{e}} \vec{\nabla} n \right) + g - r, \quad (2)$$

$$0 = \frac{dp}{dt} = -\vec{\nabla} \cdot \left(-\mu_{\text{h}} p \vec{\nabla} \phi - \frac{k_{\text{B}} T}{e} \mu_{\text{h}} \vec{\nabla} p \right) + g - r. \quad (3)$$

Please note that the two parenthesized terms on the right side of equation (2) and (3) correspond to the drift respectively diffusion of charge carriers and that the Boltzmann approximation has been used to express the latter with mobilities. All necessary steps to deduce the given equations can be found e.g. in [20]. The values of the constant parameters used in the simulations are summarized in Tab. I. The concentration of ionized donors is held constant at $3.5 \times 10^{15} \text{ cm}^{-3}$, which corresponds to the wafer's resistivity of $1.4 \Omega \text{ cm}$, whereas the ionized acceptor concentration is given by the boron density presented in Fig. 5.

The generation rate g due to the electron beam is modelled as a gaussian, where the mean value represents the position of the electron beam. The standard deviation was set to 10 nm and the amplitude to $8.87 \times 10^{25} \text{ cm}^{-3} \text{ s}^{-1}$. The recombination rate r is expressed by the following term which is motivated by a single Shockley-Read-Hall (SRH) recombination centre [21] (but omits reemission from the trap state):

$$r = (np - n_{\text{i}}^2) / (\tau_{\text{h}} n + \tau_{\text{e}} p). \quad (4)$$

This definition aims to describe an effective lifetime dominated by defects states due to the surfaces. The recombination rate is enhanced in the space charge region where carrier concentrations are low as it is the case for trap levels well inside the bandgap. Reemission is excluded as it demands for a third input parameter, i.e. the trap energy level, which is unknown in the first place. In contrast, τ_{h} and τ_{e} are defined by the experimental tails in the neutral regions shown in Fig. 4 where either n or p become clearly dominating majority carriers and set to $\tau_{\text{h}} = 1.988 \times 10^{-11} \text{ s}$ and $\tau_{\text{e}} = 7.130 \times 10^{-13} \text{ s}$. Similarities to existing approaches in the literature as well as consequences of this simplification will be discussed in detail in the next section.

The boundary conditions at the EBIC contacts in y direction are chosen to be Dirichlet conditions with $\phi = 0$, $n = n_{\text{i}}^2 / N_{\text{B,surface}}$, and $p = N_{\text{B,surface}}$ at the p-side and $\phi = k_{\text{B}} T / e \log(N_{\text{d}}^+ N_{\text{B,surface}} / n_{\text{i}}^2)$, $n = N_{\text{d}}^+$, and $p = n_{\text{i}}^2 / N_{\text{d}}^+$ at the n-side. The EBIC current is evaluated at the n-side contact. The boundary conditions in x direction are chosen to be zero flux Neumann conditions, i.e. the x component of the gradient of ϕ , n , and p are set to zero.

For the numerical implementation, COMSOL Multiphysics, Version 5.4., was used. In order to avoid boundary effects, the surface was (in accordance with the boron diffusion simulation) linearly extrapolated on the left and right side by each 500 nm during the simulation.

VI. COMPARISON OF EXPERIMENT AND SIMULATION

The previous three sections do not only present the experimental results and used numerical models, but also reflect their dependencies on each other as the position

TABLE I: Parameters in equation (1)-(4) used for the FEM simulations.

Parameter	ϵ_r	μ_e	μ_h	T	n_i	τ_h	τ_e
Value	11.7	$1100 \text{ cm}^2 \text{ V}^{-1} \text{ s}^{-1}$	$200 \text{ cm}^2 \text{ V}^{-1} \text{ s}^{-1}$	300 K	$9.802 \times 10^9 \text{ cm}^{-3}$	$1.988 \times 10^{-11} \text{ s}$	$7.130 \times 10^{-13} \text{ s}$

of the column-wise experimental EBIC maximum below the surface tip was used to fix the OED scaling factor in the boron diffusion simulation on which the numerical EBIC model was subsequently based on. Consequently, it is important to check for the model's consistency.

The experimental and simulated EBIC maps normalized to their maxima are shown in Fig. 6(a) and (b). Generally, the shape and position of the respective signals agree quite well, but small deviations exist. For the sake of a clearer presentation, exemplary vertical line profiles across the surface tip are shown in Fig. 7 together with the modulus of the electric field in equilibrium obtained from the FEM simulations. Firstly, it is worth mentioning that the EBIC signal is finite outside the SCR allowing for observations in the neutral semi-conductors. However, while the EBIC shapes agree well in the field-free regions, the experimental signal tends to be smaller inside the space charge region with larger discrepancies on the n-side. The former finding is highly consistent with previous reports about effective diffusion lengths in field-free semiconductors accounting for bulk and surface recombination simultaneously [22, 23] and confirms the choice of τ_h and τ_e as corresponding effective lifetimes. In other words, in the neutral regions, the three-dimensional TEM lamella can be described by an effective two-dimensional model successfully. Nevertheless, the recombination rate inside the SCR, i.e. in the regime where the Fermi level crosses the energy level of potential trap states, is higher in the experiment and thus requires a refinement of the model given by Equation 4 and possibly an inclusion of surface charges. Indeed, it was shown numerically in [24] that charged surface states with trap levels below resp. above the mid-gap energy influence n-type resp. p-type material more strongly which might be related to the non-symmetric discrepancies in Fig. 7. Thus, a detailed analysis if and how sensitively the density of surface charges as well as the trap level of corresponding states can be inferred from EBIC measurements should be part of future studies.

After having discussed the impact of the excess charge carrier recombination model, the focus shall be moved back to the textured geometry and the resulting boron distribution. Figure 8 shows the aluminium-silicon interface (black), the experimental (red) and simulated (blue) column-wise EBIC maxima, as well as the chemical interface (green) resulting from the boron diffusion simulation. Generally, the three latter curves agree very well and only two significant deviations are observed: Firstly, the experimental EBIC maxima tend to lower values at the left which can be explained with the linear model extrapolation neglecting the finite curvature at the edge of the scanning area shown in Fig. 3(a) and is confirmed by

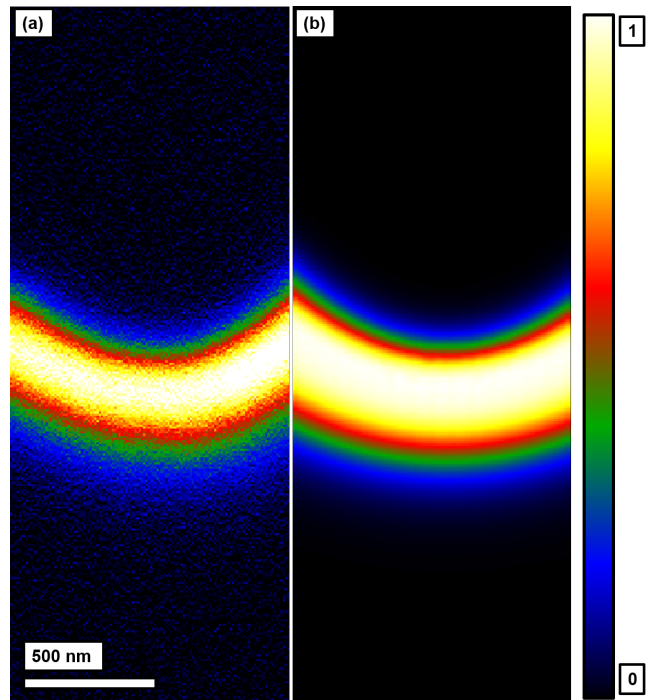


FIG. 6: (a) experimental resp. (b) simulated EBIC map normalized to their maxima.

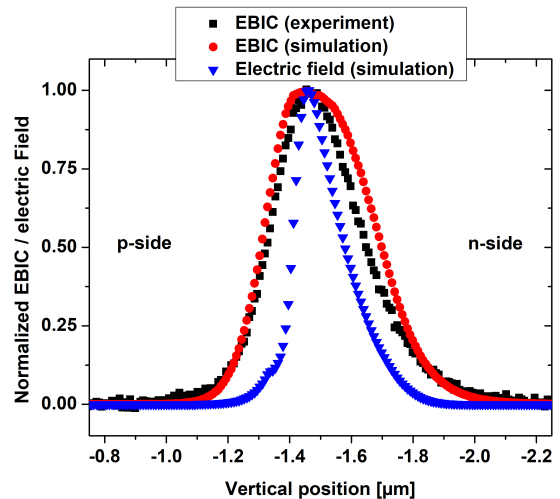


FIG. 7: Vertical profiles of the experimental (black) resp. simulated (red) normalized EBIC shown in Fig. 6(a) resp. (b) as well as the magnitude of the electric field (blue) resulting from the FEM simulation in equilibrium and normalized to its maximum. All profiles are taken across the tip of the surface texture.

the absence of similar deviations at the right. Generally, such deviations could also emerge if heterogeneities lead to boron diffusion along the electron propagation direction which is neglected in the 2D simulation. Secondly, the curvature of the EBIC maxima is slightly below the chemical junction's which reflects the lateral diffusion of excess charge carriers and leads to a mean difference of 12(2) nm between the simulated EBIC maxima and the chemical junction. In fact, the lateral diffusion gets relevant if the product of the effective diffusion length and the curvature of the chemical interface is non-negligible. Consequently, the strong influences of the surfaces are even beneficial for the sake of mapping the chemical interface, i.e. iso-concentration lines of diffusion processes, as they reduce the former. Furthermore, as indicated at the right edge, the simulated EBIC maxima shift slightly from the chemical interface (into the n-region) in the rather homogeneous case which is consistent with the findings in [25, 26]. Thus, the comparably precise coincidence of all three curves underneath the tip could result from a compensation of oppositely acting effects, i.e. the mentioned shift as well as the lateral diffusion, and in the case of larger deviations a refined pinning of the chemical junction in the boron diffusion simulation had to be used. However, given this coincidence and including only the right half of the data (and thus excluding the inaccurate linear extrapolation on the left), the mean deviation between the experimental and simulated EBIC maxima amounts to only 2(3) nm.

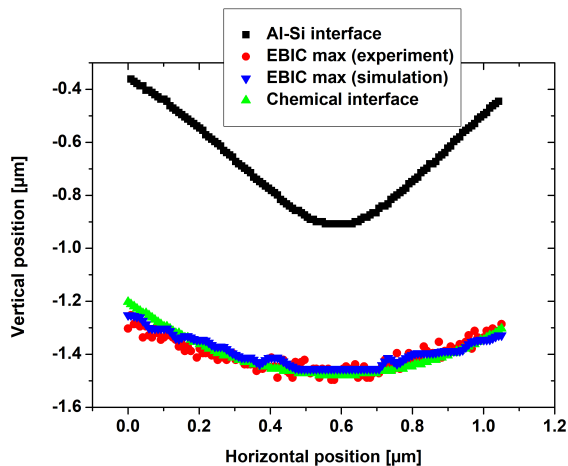


FIG. 8: Al-Si interface position (black) extracted from Fig. 3(a) as well as the column-wise maximal values of the experimental (red) and simulated (blue) EBIC maps presented in Fig. 6(a) and (b). In addition, the position of the chemical interface (green) resulting from the simulated boron concentration is plotted.

VII. CONCLUSION

In this paper, we presented a combined study of boron diffusion simulation as well as experimental and simulated scanning transmission EBIC in order to investigate the boron diffusion into a textured silicon surface. Generally, we found a good agreement between experimental and simulated EBIC by employing an effective two-dimensional FEM model and fixing the recombination parameters of the SRH-motivated term in Equation 4 in the neutral regions.

Comparing vertical EBIC profiles (Fig. 7) as well as the column-wise EBIC maxima with the chemical junction resulting from the boron diffusion (Fig. 8), three major points have been illuminated leading to following conclusions:

1. Accuracy of the recombination model inside the SCR: Clearly, there are remaining deviation between experiment and simulation. This problem is well-known from SEM-based EBIC models and has predominantly been treated numerically [24, 25, 27–29] where few experimental data points inside the SCR exist in the latter reference. Importantly, we have shown that significant EBIC signals are obtained across the entire SCR and even outside. Given the low spread of the electron beam in the sample [30], STEM-EBIC should be well-suitable to quantitatively investigate the handshake of space charge and field-free regions in future studies even if the device size approaches the nanometer scale.
2. Modelling of the surface texture: The inaccurate linear extrapolation on the left side in Fig. 8 immediately leads to significant deviations between experiment and simulation. On the one hand side, this discrepancy could have been avoided by simply extrapolating the scanning range of the EBIC map with the texture seen in the overview shown in Fig. 2. On the other hand, the deviations show once more how sensitively EBIC reflects the boron diffusion process which is why we decided to keep the linear extrapolation.
3. Lateral diffusion of excess charge carriers: In combination with the supposed shift of the maxima to the n-side in the heterogeneous case, a mean difference of 12(2) nm between the simulated EBIC maxima and the chemical junction was observed which is in contrast to the mean deviations of 2(3) nm between the experimental and simulated EBIC maxima significant. Nevertheless, as a consequence of the surfaces strongly suppressing lateral diffusion, this difference is rather small. Thus, thinning the specimen to electron transparency is even beneficial if direct conclusions about the boron concentration shall be drawn from the EBIC shape.

In summary, we have shown that STEM-EBIC allows for signal collection in- and outside the SCR of a tex-

tured silicon solar cell and that the resulting currents can be modelled by means of classical semiconductor equations. In combination with the simulation of boron diffusion, the iso-concentration line $N_B = 3.5 \times 10^{15} \text{ cm}^{-3}$ was mapped on the nanoscale which is (assuming generously a lateral resolution of 15 nm in our experiment) two orders of magnitude below the sensitivity theoretically achievable with SIMS (assuming an equivalent sputtering volume of 10^5 nm^3 [5]).

VIII. ACKNOWLEDGEMENTS

We thank Jan Verhoeven for valuable discussions about the used electronic setup as well as Thomas Lehmann for cutting the solar cell with a wafer saw to reduce its size before lamella extraction. T.M, C.F., and

M.S. are funded by the Deutsche Forschungsgemeinschaft (DFG, German Research Foundation) – 217133147/SFB 1073, project B02. V.T. is funded via the PhD Scholarship Programme of the German Federal Environmental Foundation (DBU). J.S. acknowledges funding by the State of Lower Saxony.

IX. AUTHOR CONTRIBUTIONS

T.M. conducted the experiments with support by C.F.; D.A.E. performed the EBIC and P.P. the boron diffusion simulations; V.T. prepared the macroscopic silicon solar cell under supervision of J.S.; T.M. wrote the manuscript under revision of M.S. and with contributions of P.P.; All authors read and agreed on the written paper and declare no conflicts of interest;

-
- [1] W. Shockley and H. J. Queisser, *Journal of Applied Physics* **32**, 510 (1961).
 - [2] V. Titova, D. Startsev, and J. Schmidt, in *AIP Conference Proceedings* (AIP Publishing LLC, 2018), vol. 1999, p. 040022.
 - [3] K. Singh, M. Nayak, S. Mudgal, S. Singh, and V. K. Komarala, *Solar Energy* **183**, 469 (2019).
 - [4] Y. Komatsu, D. Harata, E. W. Schuring, A. H. Vlooswijk, S. Katori, S. Fujita, P. R. Venema, and I. Cesar, *Energy Procedia* **38**, 94 (2013).
 - [5] D. McPhail, *Journal of Materials Science* **41**, 873 (2006).
 - [6] P. Pichler, *Intrinsic point defects, impurities, and their diffusion in silicon* (Springer Science & Business Media, 2012).
 - [7] D. A. Antoniadis, A. G. Gonzalez, and R. W. Dutton, *Journal of the Electrochemical Society* **125**, 813 (1978).
 - [8] S. Mirabella, D. De Salvador, E. Napolitani, E. Bruno, and F. Priolo, *Journal of Applied Physics* **113**, 3 (2013).
 - [9] F.-J. Ma, S. Dutttagupta, K. D. Shetty, L. Meng, G. S. Samudra, B. Hoex, and I. M. Peters, *Journal of Applied Physics* **116**, 184103 (2014).
 - [10] C. Cabanel, D. Brouri, and J. Laval, *The European Physical Journal Applied Physics* **34**, 107 (2006).
 - [11] P. Peretzki, B. Ifland, C. Jooss, and M. Seibt, *physica status solidi (RRL) – Rapid Research Letters* **11**, 1600358 (2017).
 - [12] T. Meyer, B. Kressdorf, J. Lindner, P. Peretzki, V. Roddatis, C. Jooss, and M. Seibt, in *Journal of Physics: Conference Series* (IOP Publishing, 2019), vol. 1190, p. 012009.
 - [13] M. Mecklenburg, W. A. Hubbard, J. J. Lodico, and B. Regan, *Ultramicroscopy* **207**, 112852 (2019).
 - [14] A. P. Conlan, G. Moldovan, L. Bruas, E. Monroy, and D. Cooper, *Journal of Applied Physics* **129**, 135701 (2021).
 - [15] V. Titova and J. Schmidt, *AIP Advances* **8**, 125023 (2018).
 - [16] T. Malis, S. Cheng, and R. Egerton, *Journal of Electron Microscopy Technique* **8**, 193 (1988).
 - [17] P. Potapov, *Ultramicroscopy* **147**, 21 (2014).
 - [18] W. Barber, C. Boynton, and P. Gallagher, *Journal of Chemical & Engineering Data* **9**, 137 (1964).
 - [19] N. Cowern, *Physical Review Letters* **99**, 155903 (2007).
 - [20] S. M. Sze and K. K. Ng, *Physics of Semiconductor Devices* (John Wiley & Sons, 2006).
 - [21] L. E. Black, *New perspectives on surface passivation: Understanding the Si-Al₂O₃ interface* (Springer, 2016).
 - [22] L. Jastrzebski, J. Lagowski, and H. Gatos, *Applied Physics Letters* **27**, 537 (1975).
 - [23] C. Donolato, *Journal of Applied Physics* **54**, 1314 (1983).
 - [24] P. M. Haney, H. P. Yoon, B. Gaury, and N. B. Zhitenev, *Journal of Applied Physics* **120**, 095702 (2016).
 - [25] M. Nichterwitz and T. Unold, *Journal of Applied Physics* **114**, 134504 (2013).
 - [26] P. Peretzki et al., *Physical Review Applied* (submitted) (2020).
 - [27] C. C. Tan, V. K. Ong, and K. Radhakrishnan, *Progress in Photovoltaics: Research and Applications* **21**, 986 (2013).
 - [28] B. Gaury and P. M. Haney, *Journal of Applied Physics* **120**, 234503 (2016).
 - [29] J. E. Moore, C. A. Affouda, S. I. Maximenko, and P. Jenkins, *Journal of Applied Physics* **124**, 113102 (2018).
 - [30] J. Goldstein, *Scanning Electron Microscopy 1977* pp. 315–324 (1977).